2

Electromagnetic interactions of charged particles with matter

2.1 Generalities on the energy loss process

The processes of transfer of part or all of its energy to a suitable medium, in which direct or indirect effects of the interaction can be recognized, mediate the detection of nuclear radiation. A variety of macroscopic mechanisms can be exploited for the conversion of the energy spent in the medium into a detectable signal: scintillation in fluorescent materials, chemical transformations intervening in photographic emulsions, condensation of droplets in saturated vapours or acoustic shock waves are just a few examples.

For charged particles, the largest fraction of energy dissipated in matter is due to electromagnetic interactions between the Coulomb fields of the projectile and of the molecules in the medium. Except for particles approaching the end of their range, where mechanical elastic collisions become relevant, the slowing down in matter is mainly due to multiple inelastic processes of excitation and ionization, whose probability is a function of the energy transfer involved. For fast electrons in condensed matter, Figure 2.1 gives an example of the dependence of the collision probability from the energy transfer. In the region between a few and a few tens of eV, the presence of atomic and molecular excitation levels with energy-dependent cross sections results in a rather complex structure: this is the region of distant collisions, since they involve a large impact parameter. Molecules can undergo radiationless rearrangements, dissociate or get excited or ionized, with the emission of photons or the appearance of free electron–ion pairs.

At increasing values of the energy transfer, the collision probability decreases exponentially with energy without particular structure up to the maximum cinematically allowed transfers, which depends on the projectile mass and energy. The outcome of these close collisions, involving increasingly small impact parameters, is the creation of excited species or the appearance of positive ions with the ejection of free electrons in the medium. Despite their low probability,

https://doi.org/10.1017/9781009291200.004 Published online by Cambridge University Press

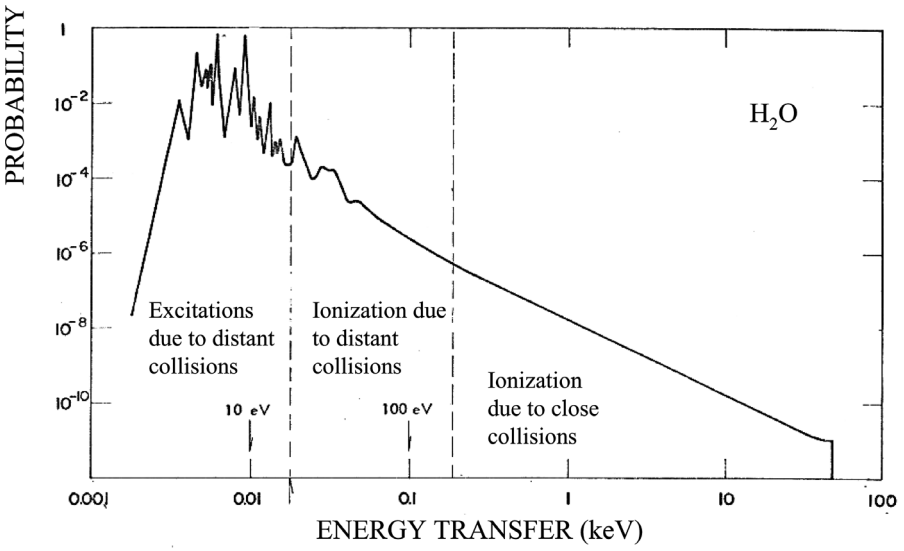


Figure 2.1 Collision probability of fast electrons in water as a function of energy transfer (Platzman, 1967). By kind permission of Elsevier.

large energy transfer yields (often named delta electrons) can further interact with the medium, and play a dominant role in determining the statistics of the energy loss process.

The number of electromagnetic collisions per unit length of material traversed, and therefore the resulting energy loss or stopping power, are a fast decreasing function of the particle velocity; on approaching the speed of light, the energy loss reaches a minimum and then slightly increases to a constant value, the so-named relativistic rise and Fermi plateau (Figure 2.2). For gases at moderate pressures, the increase can reach 40–50% above minimum, while it is reduced in condensed media.

Most of the considerations in the following sections refer to the ionization component of the energy loss; in gases, the yields of excitation processes, luminescence or scintillation photons, are usually too small in intensity to be exploitable for detection. This is not the case for heavily ionizing particles in high pressure and liquid rare gases, in which the primary scintillation is sufficiently intense to provide useful signals. Photon emission can also be enhanced by the presence of strong electric fields; the processes of primary and secondary photon emission are discussed in Chapter 5.

At very high particle energy, other mechanisms of electromagnetic interaction can occur: bremsstrahlung, coherent Cherenkov photon emission, and transition radiation. Except for electrons, for which bremsstrahlung is considerable even at low energy, these processes contribute little to the overall energy expenditure of

https://doi.org/10.1017/9781009291200.004 Published online by Cambridge University Press

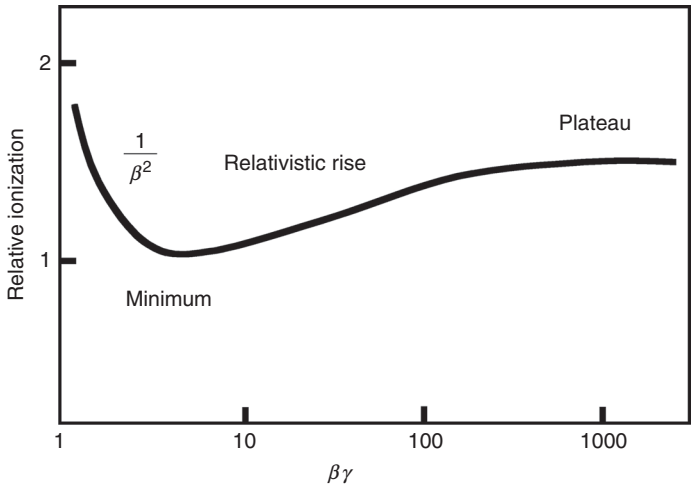


Figure 2.2 Ionization energy loss of charged particles as a function of velocity.

heavy charged particles; they can, however, be exploited for particle identification, through the detection and analysis of the angular distribution and energy spectra of emitted photons.

Electrons and photons created by the primary encounters can interact with the medium, releasing further excitations and ionizations; secondary mechanisms, particularly in composite materials, contribute to the overall photon or electron yield transferring part of the excitation energy into ionization or vice-versa. Of all outcomes of the energy loss processes, most gaseous detectors exploit the electrons created by the ionizing radiation; the presence of residual excited states, ions or photons is relevant only in that they may induce secondary phenomena, such as recombination, charge transfers and photoelectric effects. At low energies, the total specific ionization exceeds three or four times the primary, but this ratio decreases towards higher energies (Price, 1958).

Table 2.1 summarizes physical parameters useful to estimate the energy loss and ionization yields of fast charged particles in gases commonly used in proportional counters (Beringer, 2012). Data are provided at normal temperature and pressure (NTP, 20 °C and 1 atmosphere); appropriate scaling laws can be used for different conditions. The energy per ion pair W_I and the differential energy loss $\mathrm{d}E/\mathrm{d}x$ refer to unit charge particles at the ionization minimum; they correspond to reasonable averages over existing data and should be considered approximate. The same comment applies to the number of primary and total ion pairs per unit length, N_P and N_T.

The number of primary ionizations, being an outcome of independent Coulomb interactions, follows a Poisson statistics:

https://doi.org/10.1017/9781009291200.004 Published online by Cambridge University Press

Table 2.1 *Physical constants for various gases at NTP and approximate values of energy loss and ion-pair production (unit charge minimum ionizing particles).*

Gas	Density mg cm^{-3}	E_x eV	E_I eV	W_I eV	$dE/dx\|_{min}$ keV cm^{-1}	N_P cm^{-1}	N_T cm^{-1}
Ne	0.839	16.7	21.6	30	1.45	13	50
Ar	1.66	11.6	15.7	25	2.53	25	106
Xe	5.495	8.4	12.1	22	6.87	41	312
CH_4	0.667	8.8	12.6	30	1.61	37	54
C_2H_6	1.26	8.2	11.5	26	2.92	48	112
iC_4H_{10}	2.49	6.5	10.6	26	5.67	90	220
CO_2	1.84	7.0	13.8	34	3.35	35	100
CF_4	3.78	10.0	16.0	54	6.38	63	120

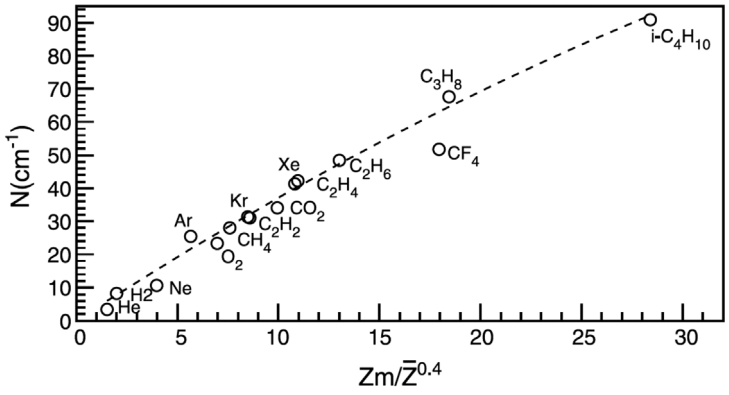


Figure 2.3 Primary ionizing collisions per cm as a function of atomic number of gases at NTP (Smirnov, 2005). By kind permission of Elsevier.

$$P_k^n = \frac{n^k}{k!} e^{-n}, \tag{2.1}$$

where n and k are the average and actual numbers of pairs, respectively.

The theoretical detector efficiency, defined as the probability of having at least one interaction, is then:

$$\varepsilon = 1 - P_0^n = 1 - e^{-n}. \tag{2.2}$$

No simple expression exists for the number of primary ionizing encounters, and one has to resort to experimentally determined data or dedicated simulation programs. For fast singly charged particles, the specific primary ionization increases almost linearly with the average charge number of the medium, as shown in the compilation of Figure 2.3 (Smirnov, 2005).

https://doi.org/10.1017/9781009291200.004 Published online by Cambridge University Press

The total number of ion pairs released in a medium in the absence of recombination or other secondary processes can be estimated from the expression:

$$N_{\mathrm{T}} = \frac{\Delta E}{W_{\mathrm{I}}}, \tag{2.3}$$

where ΔE is the total energy loss in the material; the average energy per ion pair W_{I} varies between 20 and 40 eV for most gases (see Table 2.1) and depends little on the mass and energy of the ionizing particle.

In composite materials and for the gas mixtures used in proportional counters, a composition law based on the relative concentrations can be used with good approximation, neglecting interactions between excited species; the differential energy loss in a mixture of materials *A, B,* ... with relative mass concentrations p_A, p_B, ... is then given by:

$$\frac{\Delta E}{\Delta x} = p_A\left[\frac{\Delta E}{\Delta x}\right]_A + p_B\left[\frac{\Delta E}{\Delta x}\right]_B + \ldots . \tag{2.4}$$

As an example, the average energy loss and ionization density for a relativistic charged particle in a gaseous counter filled with a mixture of argon–isobutane in the mass proportions 70–30, at normal conditions, from the table and using the appropriate composition laws, are $\Delta E = 3.5$ keV/cm, $N_{\mathrm{P}} = 45$ ion pairs/cm, $N_{\mathrm{T}} = 136$ ion pairs/cm; the average distance between primary ionizing collisions is about 220 μm, and each primary interaction cluster contains three ion pairs. These are of course average numbers; the actual statistical distribution of the yields will be discussed later.

2.2 The Bethe–Bloch energy loss expression

The energy loss processes due to multiple Coulomb interactions of charged particles have been subject of research since the original works of Rutherford on heavy particle scattering. In a semi-classical formulation, usually referred to as the Rutherford expression, the probability of a unit charge particle of velocity β to release an energy between ε and $\varepsilon+\mathrm{d}\varepsilon$ in a layer of a material of thickness $\mathrm{d}x$ and density ρ can be written as:

$$\frac{\mathrm{d}^2N}{\mathrm{d}x\,\mathrm{d}\varepsilon} = K\frac{Z}{A}\frac{\rho}{\beta^2}\frac{1}{\varepsilon^2} \qquad K = \frac{4\pi Ne^2}{mc^2}. \tag{2.5}$$

e and m are the charge and mass of the electron, Z, A and ρ the medium atomic number, mass and density, and N Avogadro's number; in the CGS system of units the rest mass of the electron $mc^2 = 0.511$ MeV and $K = 0.308$ MeV g^{-1} cm^2.

https://doi.org/10.1017/9781009291200.004 Published online by Cambridge University Press

Expression (2.5) describes well the energy loss process of ions for intermediate velocities. Several corrections are, however, necessary both at low and very high velocities to obtain agreement with the experimental results (Fano, 1963; Northcliffe, 1963). In a general formulation the differential energy loss, or stopping power (Bethe–Bloch expression) is written as:

$$\frac{\Delta E}{\Delta x} = -\rho \frac{2KZ}{A\beta^2}\left[\ln \frac{2mc^2\beta^2}{I(1-\beta^2)} - \beta^2 - \frac{C}{Z} - \frac{\delta}{2}\right]. \tag{2.6}$$

The expression shows that the differential energy loss depends only on the particle's velocity β and not on its mass; the additional term C/Z represents the so-called inner shell corrections, that take into account a reduced ionization efficiency on the deepest electronic layers due to screening effects, and $\delta/2$ is a density effect correction arising from a collective interaction between the medium and the Coulomb field of the particle at highly relativistic velocities; its contribution is small for non-condensed media. It should be noted, however, that in thin absorbers electrons produced with high momentum transfer might escape from the layer, thus reducing the effective yield.

No simple analytical expression for the correction factors in expression (2.6) has been given; tables and compilations allow their estimate (Gray, 1963; Fano, 1963; Northcliffe, 1963). Alternatively, one can find tables and plots of energy loss for ions in both the low and intermediate (Williamson and Boujot, 1962; Ziegler, 1977) and the high energy regions (Trower, 1966). Web-based platforms permit one to compute stopping powers and ranges of charged particles in a wide range of materials and energies (Berger *et al.*, 2011). Expressing the material thickness in reduced units (length times density), the stopping power is around 2 MeV cm^2g^{-1} almost independently from the material, with the exception of very light materials, as shown in Figure 2.4 (Beringer, 2012).

Expressed as a function of momentum, the average energy loss depends on the mass of the particle; this can be exploited for particle identification, as discussed in the next section. An example is shown in Figure 2.5 for an argon–CO_2 mixture at atmospheric pressure (Allison *et al.*, 1974).

2.3 Energy loss statistics

The differential energy loss computed with the Bethe–Bloch expression or obtained from the described compilations represents only the average; event per event values fluctuate around the average, with a distribution that depends on the particle energy and the absorbing medium nature, thickness and conditions. The process is dominated by the statistics of emission of energetic delta electrons;

https://doi.org/10.1017/9781009291200.004 Published online by Cambridge University Press

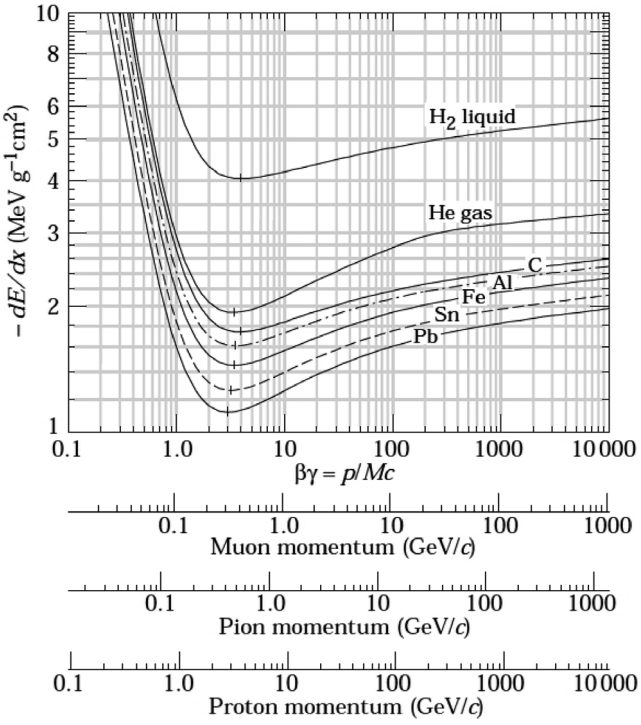


Figure 2.4 Differential energy loss as a function of velocity and momentum for singly charged particles in different materials (Beringer, 2012). By kind permission of the American Physical Society.

the simulation programs mentioned in the previous section can describe it in detail. However, it is instructive to use a simple formulation derived from Rutherford's approximation. Assuming that all energy in an interaction is imparted to a quasi-free electron, integration of expression (2.5) between ε_0 and ε_M (the maximum energy transfer) gives the probability of creating in a layer dx an electron of energy equal or larger than ε_0:

$$\frac{dN(\varepsilon > \varepsilon_0)}{dx} = W\left(\frac{1}{\varepsilon_0} - \frac{1}{\varepsilon_M}\right) \cong \frac{W}{\varepsilon_0}, \quad W = K\frac{Z}{A}\frac{1}{\beta^2}, \tag{2.7}$$

an approximation valid for $\varepsilon_M \gg \varepsilon_0$.

A comparison between the probability deduced from this expression and the result of a more sophisticated quantum-mechanical Monte Carlo calculation is shown in Figure 2.6 (Lapique and Piuz, 1980); the second shows clearly the contribution of the various electronic shells levels. For many practical purposes, however, the simpler formulation is often good enough.

https://doi.org/10.1017/9781009291200.004 Published online by Cambridge University Press

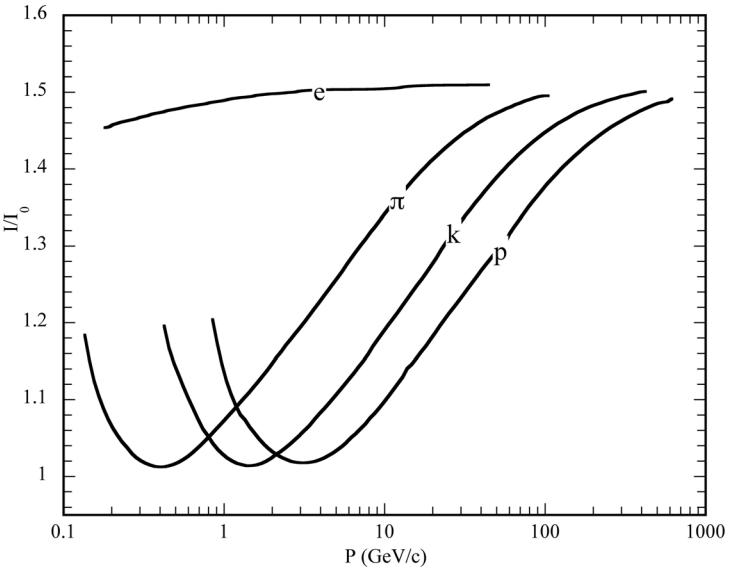


Figure 2.5 Mass dependence of the average specific ionization as a function of the particle momentum in the relativistic rise region (Allison *et al.*, 1974). By kind permission of Elsevier.

As an example, in one cm of argon at STP there is a ~5% probability of emission of an electron of energy equal to or larger than 2 keV; this has to be compared with the average energy loss of 2.4 keV/cm in the same conditions (see Table 2.1), meaning that in 5% of the events the observed energy loss is almost twice the average.

The production of energetic secondary (delta) electrons, with low probability but large ionization yields, determines the peculiar shape of the energy loss distribution; named the Landau expression, from the Russian physicist who studied the process in the forties, it can be written as:

$$f(\lambda) = \frac{1}{\sqrt{2\pi}} e^{-\frac{1}{2}(\lambda + e^{-\lambda})}, \tag{2.8}$$

where the energy variable λ represents the normalized deviation from the most probable energy loss $(\Delta E)_{\mathrm{MP}}$:

$$\lambda = \frac{\Delta E - \Delta E_{\mathrm{MP}}}{\xi}, \quad \xi = K \frac{Z}{A} \frac{\rho}{\beta^2} x.$$

For thin gas samples, the width of the energy loss distribution is close to the most probable value, with a characteristic asymmetric tail at large values. In Figure 2.7 (Igo *et al.*, 1952), values measured with a proportional counter are compared with

https://doi.org/10.1017/9781009291200.004 Published online by Cambridge University Press

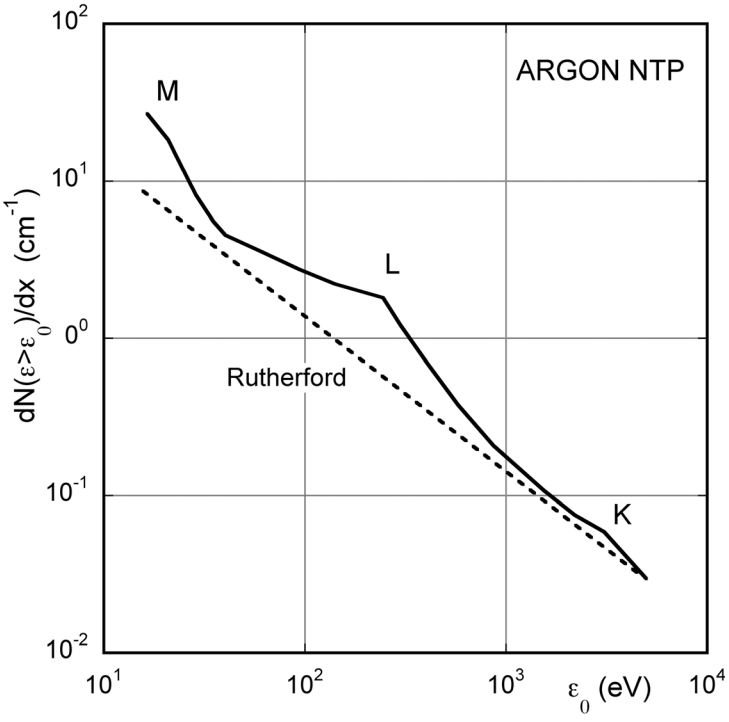


Figure 2.6 Number of electrons produced by ionization at an energy equal to or larger than ε_0; the full curve is a Monte Carlo calculation, the dashed line the prediction of Rutherford theory (Lapique and Piuz, 1980). By kind permission of Elsevier.

Landau's prediction, showing a good concordance; dedicated studies and refinements of the theory have since improved the agreement. In the figure, the dashed curve is the expected distribution for a Gaussian statistics, i.e. only determined by the fluctuations in the number of primary ionization encounters.

Figure 2.8 (Lehraus *et al.*, 1981) gives an example of energy loss distribution measured with a thin gaseous counter for particles of different mass (protons and electrons) and equal momentum. As expected, the most probable values differ by about 30%, but the distributions largely overlap due to the Landau energy loss statistics. To achieve particle identification, multi-sampling devices are used to measure many independent segments of the same tracks and combine them with appropriate statistical analysis; a truncated mean algorithm on 64 measured samples results in the distributions shown in Figure 2.9, with a good separation between protons and pions and, to a lesser extent, electrons (Lehraus *et al.*, 1981).

Motivated by the development of multi-wire chamber arrays for relativistic particle identification, systematic measurements have been made to find gas

https://doi.org/10.1017/9781009291200.004 Published online by Cambridge University Press

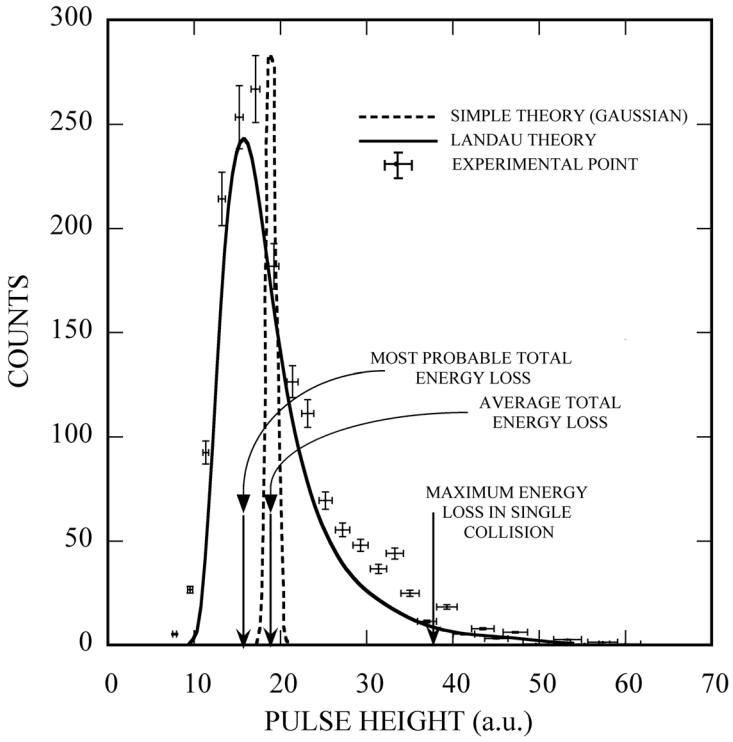


Figure 2.7 Comparison of experimental data (points with error bars) and Landau theory calculations of the energy loss in a thin sample of gas. The dashed curve represents the Gaussian expectation for the same average energy loss (Igo *et al.*, 1952). By kind permission of the American Physical Society.

mixtures with the best resolution. A compilation of results is given in Figure 2.10, providing the relative resolution (FWHM/most probable energy loss) in a wide range of gases and as a function of sample thickness (Lehraus *et al.*, 1982). As shown also in Figure 2.11, from the same reference, the best resolution is obtained with hydrocarbons; unfortunately, in light molecular gases the relativistic rise is smaller than for the noble gases, balancing the improvements due to resolution. In consideration also of their flammability and tendency to create deposits under irradiation (see Chapter 16), the use of hydrocarbons gas fillings has been basically abandoned, except in small percentages.

A model for the calculation of ionization losses of relativistic particles in thin absorbers, with comparison to experimental results, is given in Grishin *et al.* (1991).

Using an improved photo-absorption ionization model, Smirnov (2005) has computed the distribution of the energy loss of fast particles in a range of conditions and compared the results with experimental measurements; the program

https://doi.org/10.1017/9781009291200.004 Published online by Cambridge University Press

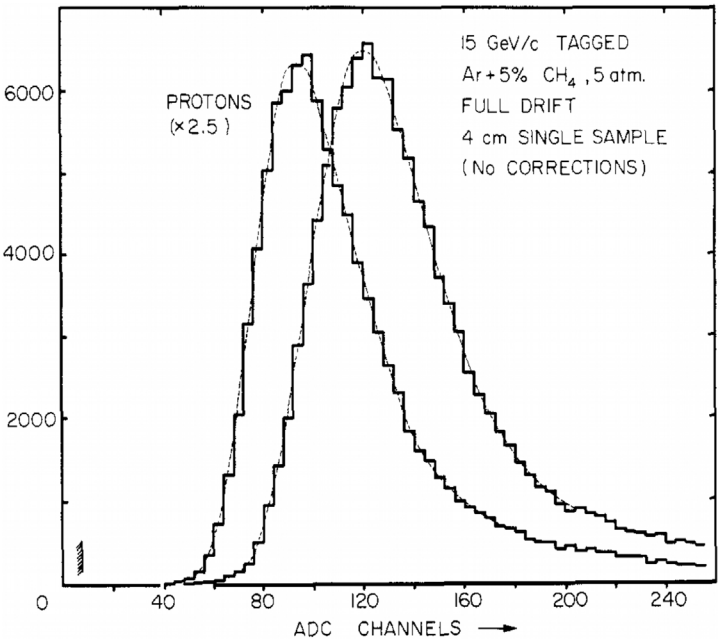


Figure 2.8 Experimental energy loss spectra in a thin sample of gas for protons and pions of equal momentum (15 GeV/c) (Lehraus *et al.*, 1981). © The Royal Swedish Academy of Sciences. By kind permission of IOP Publishing.

HEED, available on-line, allows one to compute the energy loss processes in a wide range of conditions (Smirnov, 2012). The agreement is excellent, as shown in Figure 2.12 and Figure 2.13, providing the energy loss for pions and electrons, in the region of the relativistic rise, as a function of the particle velocity and for several model calculations.

The probability of a primary ionization center consisting of several secondary ion–electron pairs, or cluster size, can be computed with the programs mentioned above, or directly measured; it is a fast decreasing function of the number of charges in the cluster, and depends little on the medium. Figure 2.14 shows measured values for argon and methane (Fischle *et al.*, 1991).

Attempts have been devised to exploit the primary ionization information, a method named cluster counting, that would allow one to improve considerably the particle identification resolution (Walenta, 1981). The experimental problem is to preserve the structure of the primary clusters during their drift to a collecting electrode, since the cloud is quickly smeared by diffusion. In the time expansion chamber (TEC), described in Section 9.5, this is partly achieved with a suitable optimization of the gas mixture having low drift velocities at moderate electric fields. The primary clusters distribution for relativistic particles,

https://doi.org/10.1017/9781009291200.004 Published online by Cambridge University Press

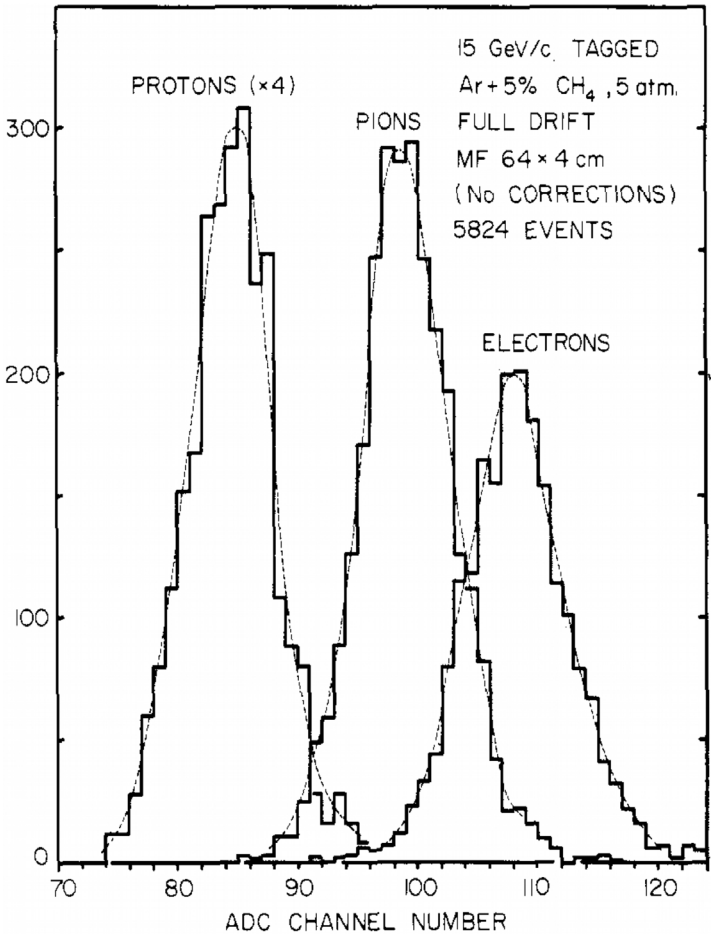


Figure 2.9 Particle identification resolution obtained from statistical analysis of energy loss measured on 64 track samples (Lehraus *et al.*, 1981). © The Royal Swedish Academy of Sciences. By kind permission of IOP Publishing.

measured with a TEC prototype, exhibits a Poisson-like shape, as against a Landau distribution that would result when recording the total ionization loss (Walenta, 1979).

By operating a drift chamber with helium-containing gas fillings to increase the distance between clusters, some efforts to improve on particle identification resolution at high energies have met a moderate success (Cerrito *et al.*, 1999).

Model calculations suggested, however, that the primary ionization increase in the relativistic rise region is only a fraction of the total, as shown in Figure 2.15, demonstrating that an important fraction of the relativistic rise is produced by the

https://doi.org/10.1017/9781009291200.004 Published online by Cambridge University Press

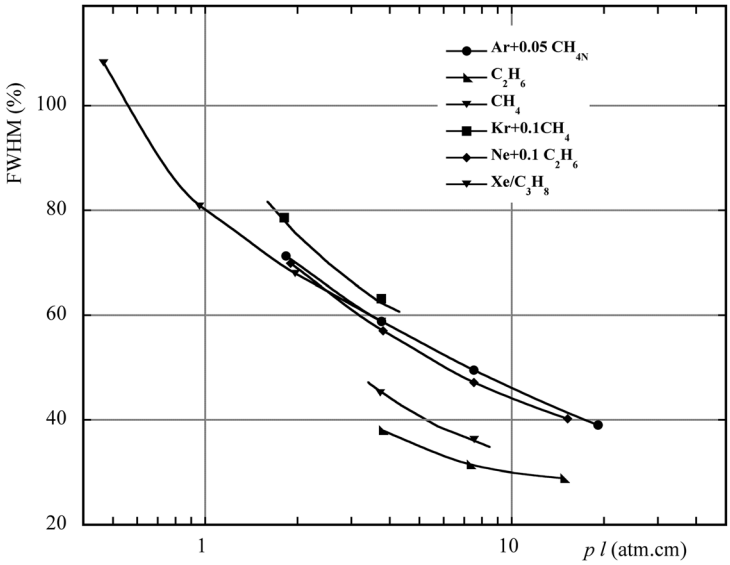


Figure 2.10 Resolution of the ionization energy loss of fast particles for several gases, as a function of the sample thickness given in atm.cm (Lehraus *et al.*, 1982). By kind permission of Elsevier.

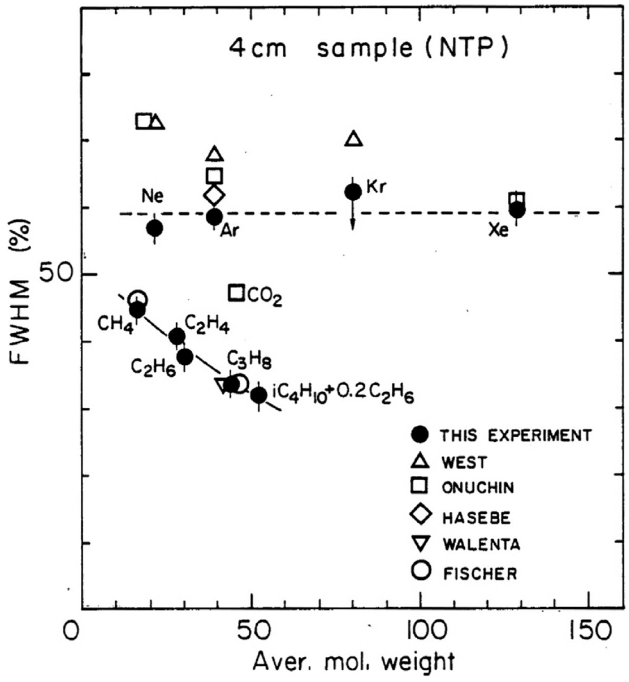


Figure 2.11 Relative ionization energy loss resolution in several gases in 4 cm gas samples (Lehraus *et al.*, 1982). By kind permission of Elsevier.

https://doi.org/10.1017/9781009291200.004 Published online by Cambridge University Press

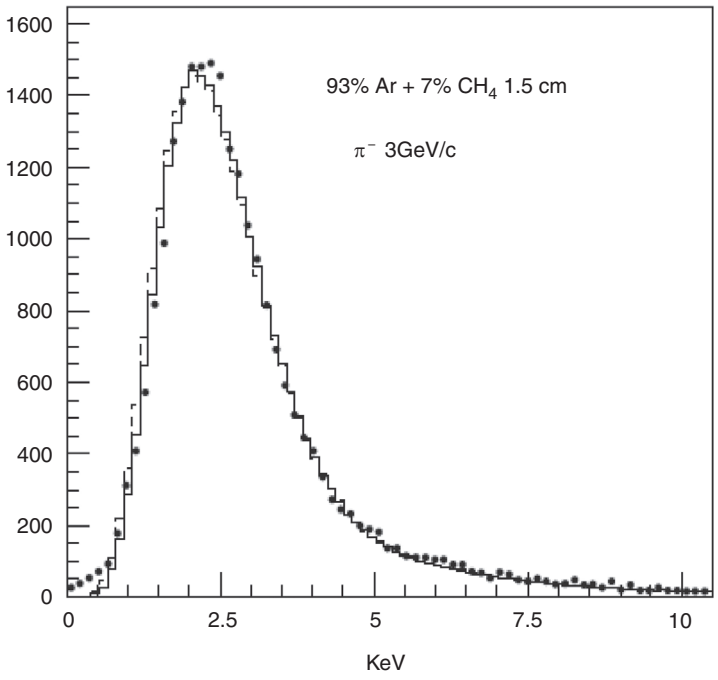


Figure 2.12 Comparison between measured and computed energy loss distributions (Smirnov, 2005). By kind permission of Elsevier.

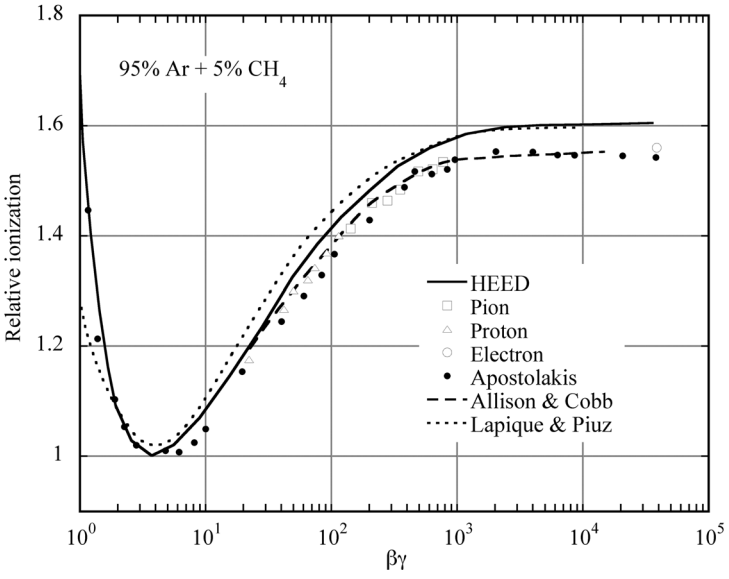


Figure 2.13 Relative most probable ionization loss measured and computed with several models (Smirnov, 2005). By kind permission of Elsevier.

https://doi.org/10.1017/9781009291200.004 Published online by Cambridge University Press

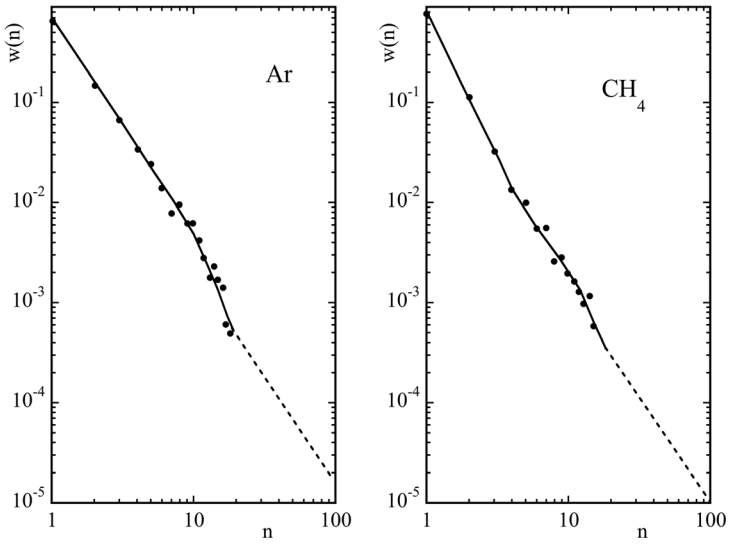


Figure 2.14 Cluster size probability for fast particles in argon and methane (Fischle *et al.*, 1991). By kind permission of Elsevier.

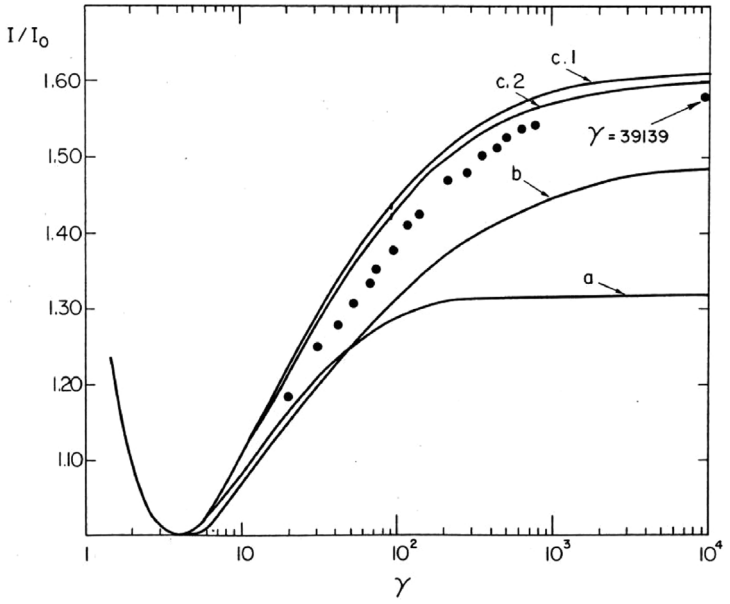


Figure 2.15 Relative ionization computed for the total losses under slightly different assumptions (c1 and c2), for the number of primary clusters (a) and the mean number of released electrons (b). The dots represent an experimental measurement. (Lapique and Piuz, 1980). By kind permission of Elsevier.

https://doi.org/10.1017/9781009291200.004 Published online by Cambridge University Press

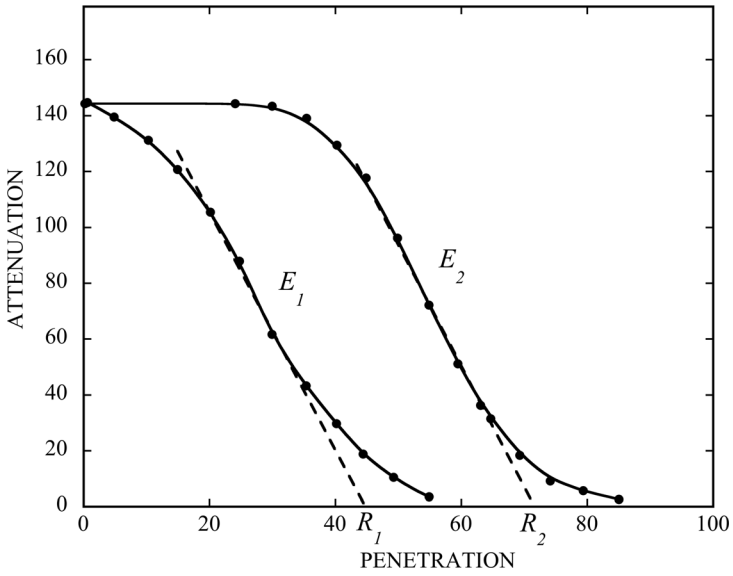


Figure 2.16 Definition of the practical electron range from attenuation curves.

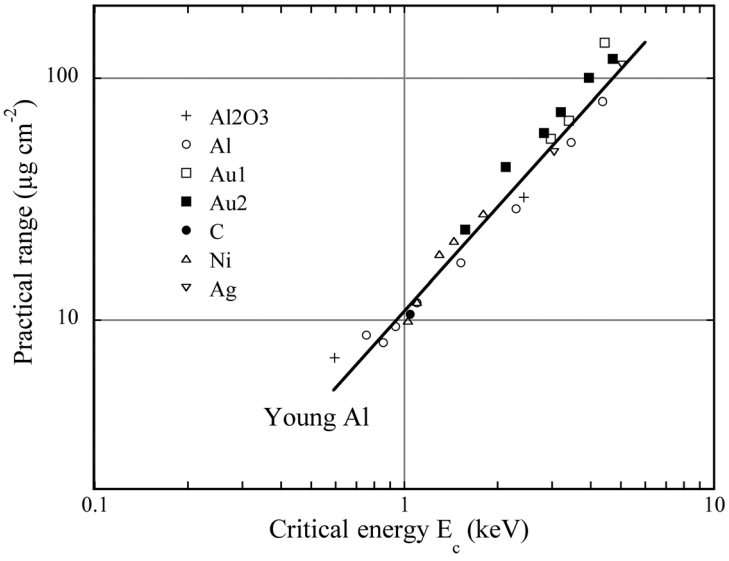


Figure 2.17 Practical electron range as a function of energy in several materials (Kanter, 1961). By kind permission of the American Physical Society.

secondary delta electrons produced by primary encounters; this reduces the possible advantages of the improved statistics and brings the expected resolution of the cluster counting technique close to the one of a simpler total ionization loss measurement (Lapique and Piuz, 1980).

https://doi.org/10.1017/9781009291200.004 Published online by Cambridge University Press

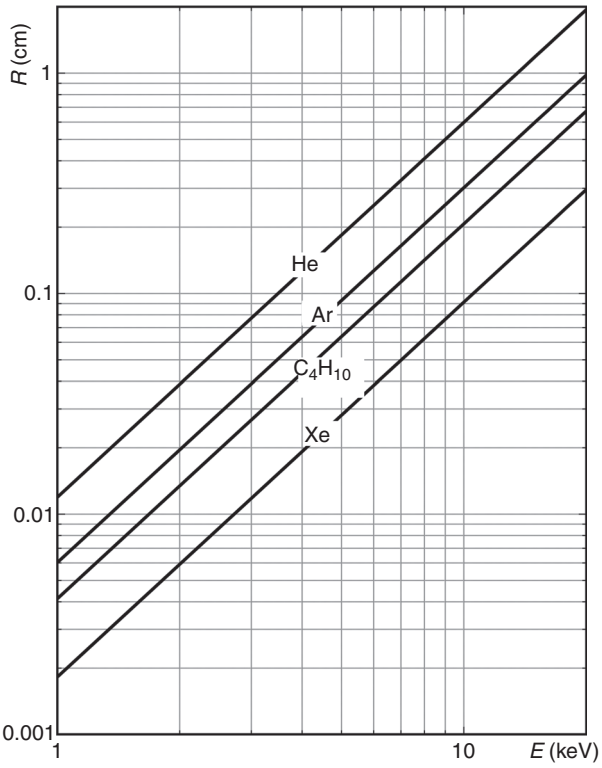


Figure 2.18 Approximate electron range in gases at NTP as a function of their energy.

2.4 Delta electron range

A consequence of the delta electron statistics is the smearing of the ionization trails outside the line of flight of the particle; this can be a limiting factor in the localization capabilities of detectors, in general only recording the average position of the ionization clouds (Sauli, 1978).

Due to multiple scattering with the gas molecules, slow electrons do not follow straight trajectories; the average distance from the emission point, or practical range, is shorter than the integrated path length. The practical range for a given energy is defined from the extrapolation to the abscissa of the attenuation curve at increasing absorber thickness, as shown schematically in Figure 2.16 for two mono-energetic beams of electrons. Expressed in reduced units, the practical range for slow electrons in light materials is almost independent of the element, as seen in the compilation of Figure 2.17 (Kanter, 1961).

For slow electrons (between 1 and 40 keV), a good approximation of the electrons' practical range in light elements is given by:

$$R = 10.0\, E^{1.7}, \tag{2.9}$$

https://doi.org/10.1017/9781009291200.004 Published online by Cambridge University Press

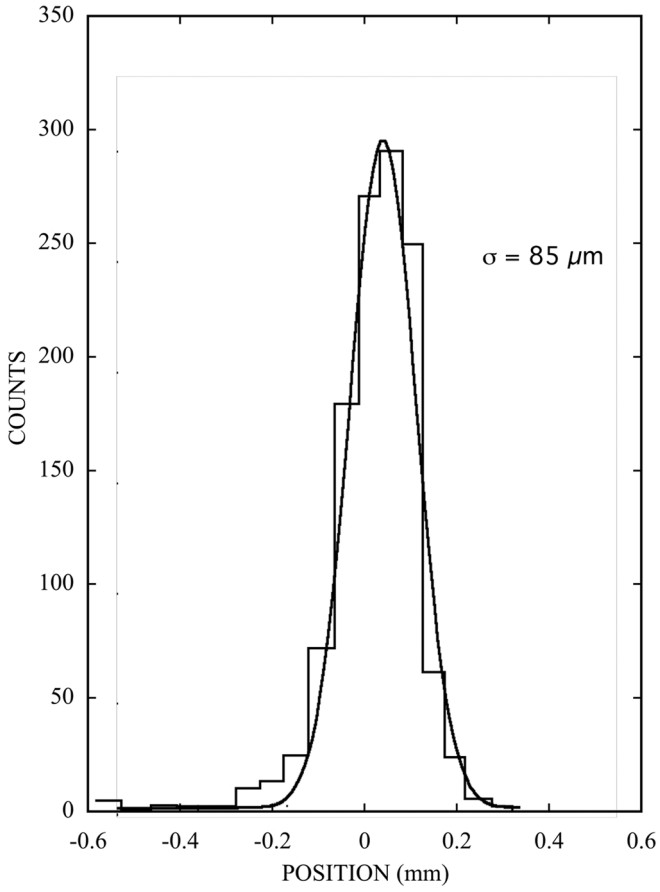


Figure 2.19 Localization accuracy in drift chambers, showing larger deviations at short drift times due to ionization produced by long-range delta electrons (Breskin *et al.*, 1974b). By kind permission of Elsevier.

with R in μg cm^{-2} and E in keV (Kobetich and Katz, 1968). Figure 2.18 gives the electron range in several gases at NTP computed from the expression; in argon, a 2 keV electron has a practical range of 180 μm. As indicated in the previous section, an electron of at least this energy is produced in 5% of the events; for those tracks, a corresponding systematic shift of the measured position is expected, contributing to the tails in the distributions, compared with typical localization error of 50–100 μm achieved with high accuracy drift chambers (Breskin *et al.*, 1974b). An example is shown in Figure 2.19, providing the measured drift time distribution in the detector for tracks perpendicular to the drift direction; the asymmetric tail on the left side is due to the earlier arrival of the charge released by long-range delta electrons, and corresponds to about 5% of the events.

https://doi.org/10.1017/9781009291200.004 Published online by Cambridge University Press

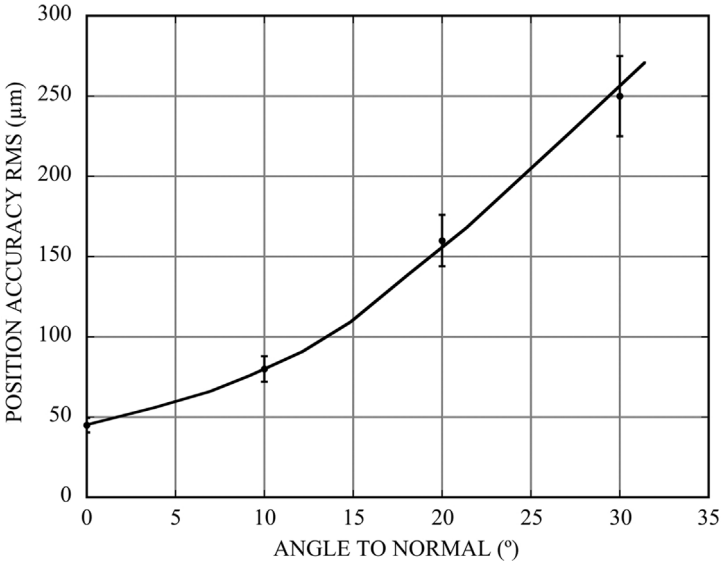


Figure 2.20 Angular dependence of the localization accuracy measured with the cathode induced charge method (Charpak *et al.*, 1979b). By kind permission of Elsevier.

A similar dispersive effect is observed in detectors exploiting the measurement of the cathode-induced charge profile; asymmetries in the energy loss result in a strong dependence of the localization accuracy on the incidence angle of tracks, see Section 8.9; an example is shown in Figure 2.20 (Charpak *et al.*, 1979b). The two dispersive effects add up in devices exploiting both the drift time and the induced charge measurements, as the time projection chambers (Chapter 10).

Use of heavier gases or higher pressures helps reduce the range of electrons of a given energy, but may be compensated by the increase in their number.

https://doi.org/10.1017/9781009291200.004 Published online by Cambridge University Press